Journal of Photochemistry and Photobiology A: Chemistry 199 (2008) 230–235

Contents lists available at ScienceDirect

Journal of Photochemistry and Photobiology A: Chemistry

journal homepage: www.elsevier.com/locate/jphotochem

New molten-salt synthesis and photocatalytic properties of $La_2Ti_2O_7$ particles

David Arney, Brittany Porter, Benjamin Greve, Paul A. Maggard *

Department of Chemistry, North Carolina State University, Raleigh, NC 27695–8204, USA

ARTICLE INFO

Article history:
Received 3 January 2008
Received in revised form 24 May 2008
Accepted 2 June 2008
Available online 20 June 2008

Keywords:
Flux synthesis
$La_2Ti_2O_7$
Photocatalysis

ABSTRACT

The (1 1 0)-layered perovskite $La_2Ti_2O_7$ photocatalyst has been synthesized in high purities and in homogeneous microstructures within a molten Na_2SO_4/K_2SO_4 flux in short reaction times of ~1–10 h. The $La_2Ti_2O_7$ particle morphologies and sizes were investigated as a function of flux amounts (flux:$La_2Ti_2O_7$ molar ratios of 1:1, 2:1, 5:1, and 10:1) and reaction times (1, 2, 5, and 10 h). Powder X-ray diffraction confirmed the structure type and high purity, and UV–vis diffuse reflectance measurements yielded optical bandgap sizes of ~3.75–3.81 eV. Rectangular platelet morphologies are obtained with maximal dimensions of ~500–5000 nm, but with thicknesses down to <100 nm, and which decrease in size with increasing amounts of flux used in the synthesis. Photocatalytic activities of the $La_2Ti_2O_7$ products were measured under ultraviolet irradiation in aqueous methanol solutions and yielded rates for hydrogen production from 55 to 140 μmol H_2 h^{-1} g^{-1}, with the maximum photocatalytic rates for the smallest particles, e.g. for 1:1 and 10:1 flux:$La_2Ti_2O_7$ ratios respectively. The flux-prepared $La_2Ti_2O_7$ products were also photocatalytically active in pure deionized water, yielding maximal rates for hydrogen formation of 31 μmol H_2 h^{-1} g^{-1}. The observed photocatalytic rates were up to nearly two times greater than that obtained when $La_2Ti_2O_7$ was prepared by the reported solid-state method, and indicate that the exposed crystallite edges and the (0 1 0) and (0 0 1) crystal faces play a key role in the photocatalysis mechanisms for hydrogen formation.

1. Introduction

The synthesis of early transition-metal oxide particles has drawn considerable recent attention owing to their absorption of ultraviolet/visible light and efficient photocatalytic production of H_2 and O_2 from aqueous solutions [1–4]. Typically, the metal oxides are also loaded with surface co-catalyst islands, such as RuO_2 or Pt particles, and more recently Rh/Cr_2O_3 core–shell particles [5], that function to assist the electron transfer and liberation of H_2/O_2 upon irradiation in solution. Among the many explored titanate, niobate, and tantalate photocatalysts, solids with layered types of structures have generally been among those exhibiting the highest photocatalytic rates, such as most prominently known for the (1 1 0) layered perovskites including $M_2Nb_2O_7$ (M=Ca, Sr), $R_2Ti_2O_7$ (R=Y, La–Yb) and $La_4CaTi_5O_{17}$ [6,7]. The reported quantum yields of the (1 1 0) layered perovskites range as high as ~20–50% at ultraviolet wavelengths [4,7]. Of these layered perovskites, $La_2Ti_2O_7$ has received the most attention because of its photocatalytic activity in the presence of sacrificial reagents or in pure water. Its photocatalytic activity for H_2 and/or O_2 production from aqueous solutions has been studied as a function of different rare-earth (R) elements (i.e. $R_2Ti_2O_7$) [8–10], with transition-metal dopants for its sensitization to visible light [11,12], as well as for the decomposition of organic pollutants [13,14]. High photocatalytic activities for metal oxides have generally been correlated with smaller particle sizes and with good particle crystallinity. However, the standard solid-state synthesis of $La_2Ti_2O_7$ typically yields low surface areas and requires high temperatures (~1100–1400 °C) and repeated regrindings and reheatings owing to the difficulty of achieving good homogeneity and high purity by this method. Relatively few alternative preparative routes to $La_2Ti_2O_7$ have been explored, including hydrothermal syntheses [15,16] and the high-temperature decomposition of metal-organic precursors [17,18]. These syntheses have provided for smaller particle sizes compared to the solid-state method, but also typically require extended heating times and multi-step synthetic procedures.

Our research efforts in this area have focused on the rapid and simple single-step synthesis (down to ~1–2 h) of metal-oxide photocatalysts within molten-salt fluxes. For example, we recently reported the first flux synthesis of high purity $Bi_5Ti_3FeO_{15}$ and $LaBi_4Ti_3FeO_{15}$ with highly textured platelet-like particle sizes that can be controlled from <1 to >20 μm, and that are obtained in only 0.5–1 h at 800 or 900 °C [19]. We have also demonstrated that these methods allow for the visible-light sensitization of layered

* Corresponding author. Tel.: +1 919 515 3616; fax: +1 919 515 5079.
E-mail address: Paul_Maggard@ncsu.edu (P.A. Maggard).

1010-6030/$ – see front matter © 2008 Elsevier B.V. All rights reserved.
doi:10.1016/j.jphotochem.2008.06.005

perovskite metal oxides via rapid flux-assisted exchange reactions [20]. However, the effect of flux synthesis on the photocatalytic activity of layered metal oxides has not been investigated to date. By comparison, the flux synthesis of a perovskite-type photocatalyst, La-doped $NaTaO_3$, was found to result in up to a two-fold enhancement of photocatalytic rates, and which was a function of the particle sizes and fine surface features [21]. A flux-synthesis route to the (1 1 0) layered perovskite photocatalyst $La_2Ti_2O_7$ would be promising for control over the particle-size distributions and homogeneity, and therefore could enable the study of the underlying particle features and surfaces that control its photocatalytic properties.

Presented herein is the new flux synthesis of $La_2Ti_2O_7$ and an investigation of the effect of its particle sizes/morphologies on optical properties and photocatalytic rates for hydrogen formation. The reaction durations and reactant-to-flux ratios were independently varied, and both of which can affect the particle sizes and aggregation. The products were characterized by powder X-ray diffraction (PXRD), UV–vis diffuse reflectance spectroscopy, and scanning electron microscopy. Photocatalytic activities were measured in an aqueous methanol as well as pure water solutions, both in order to evaluate the effect of particle sizes and morphologies on the rate of H_2 formation and for comparisons to the solid-state products.

2. Experimental

2.1. Synthesis and characterization

The flux synthesis of $La_2Ti_2O_7$ was performed by combining a stoichiometric mixture of AR grade TiO_2 and La_2O_3 (preheated and dried at 900 °C), which was ground together with ~10 ml of acetone. After evaporation of the acetone, the reactants were combined with the Na_2SO_4/K_2SO_4 (1:1 molar ratio) salt flux to give flux:$La_2Ti_2O_7$ molar ratios of 1:1, 2:1, 5:1, and 10:1. These reactant mixtures were then placed inside an alumina crucible and heated at 1100 °C inside a box furnace for reaction times of 1, 2, 5, and 10 h. The crucibles were allowed to radiatively cool to room temperature and the resulting products were washed with hot deionized water to remove the flux and then dried overnight in an oven at 80 °C. A fine homogeneous white powder of $La_2Ti_2O_7$ was obtained in high purity, as judged from powder X-ray diffraction. The solid-state preparation of $La_2Ti_2O_7$ involved grinding, pelletizing, and heating the La_2O_3 and TiO_2 reactants at 1100 °C for 50 h with one intermittent grinding, similar to other reported procedures [8]. High-resolution powder X-ray diffraction patterns of all products were collected on an INEL diffractometer using Cu $K\alpha_1$ (λ = 1.54056 Å) radiation from a sealed-tube X-ray generator (35 kV, 30 mA) using a curved position sensitive detector (CPS120). Scanning electron microscopy (SEM) was performed using a JEOL JEM 6300 in order to examine the particle microstructures and approximate sizes of the reaction products. UV–vis Diffuse Reflectance Spectra (DRS) were collected on powdered samples using a CARY 3E spectrophotometer equipped with an integrating sphere.

2.2. Photocatalytic measurements

Measurements of the photocatalytic rates of the flux-synthesized $La_2Ti_2O_7$ products were conducted similar to previously described procedures [20–23]. Each sample was first loaded with 1 wt.% platinum co-catalyst by the photodeposition method. The platinum co-catalyst serves as a well-known kinetic aid in solution for the reduction of H_2O at the surfaces to give H_2. First, 100 mg of $La_2Ti_2O_7$ was mixed with 30 ml of an aqueous solution of dihydrogen hexachloroplatinate(IV) ($H_2PtCl_6{\cdot}6H_2O$; Alfa Aesar, 99.95%), and that was then irradiated using a 400 W Xe arc-lamp with constant stirring for 2 h. The remaining amount of un-deposited Pt salt left in solution after this step was <0.5%, as determined from UV–vis measurements. After platinization, the grayish-colored $La_2Ti_2O_7$ particles were separated via centrifugation, washed with distilled water to remove any remaining Cl^- ions, and then dried in an oven at 80 °C. Next, a weighed (100 mg) amount of the platinized $La_2Ti_2O_7$ was added to an ~90 ml quartz reaction vessel that was then filled with a 20% aqueous methanol solution, or alternatively, with pure water. The added methanol functions as a hole scavenger, thereby generating CO_2 from photo-oxidation, and which allows the measurement of the formation rate of H_2 alone and without the typically more rate-limiting step of O_2 formation. The photoreaction vessel was connected to a small horizontal quartz tube that trapped the evolved gases, and contained a moveable liquid bubble that allowed a volumetric determination of the amount of evolved gases at a constant pressure. The metal-oxide particles were stirred in the dark for ~1–2 h to remove any trapped gases on the particles surfaces. Next, this outer-irradiation type quartz reaction cell was irradiated under constant stirring using a 1000 W Xe arc-lamp equipped with an IR water filter and cooled using an external fan. Each of the photocatalytic reactions exhibited the formation of copious amounts of gases that rose to the top of the reaction cell, and that was consistent with the movement of the liquid bubble. The progress of the photocatalytic reactions was marked every hour and used to calculate the amount of gases generated. The trapped gasses were injected into a gas chromatograph (SRI MG #2, helium ionization and thermal conductivity detectors) in order to identify the formed gases as H_2 and CO_2, and to confirm a constant molar ratio over time.

3. Results and discussion

The $La_2Ti_2O_7$ solid crystallizes in a structure containing (1 1 0) perovskite layers spanning four TiO_6 octahedra in width, and which stack together in the monoclinic and polar space group $Pna2_1$ [24]. The PXRD patterns of the flux products, shown in Fig. 1, could be fitted and indexed to the $La_2Ti_2O_7$ structure and confirm that high purity and good crystallinity could be obtained in short reaction times of 1–10 h within a Na_2SO_4/K_2SO_4 flux (1:1 molar ratio) at flux:$La_2Ti_2O_7$ ratios of 1:1, 2:1, 5:1 and 10:1. To evaluate the particle sizes and morphologies of the $La_2Ti_2O_7$ products, scanning electron microscopy images were taken on the samples prepared

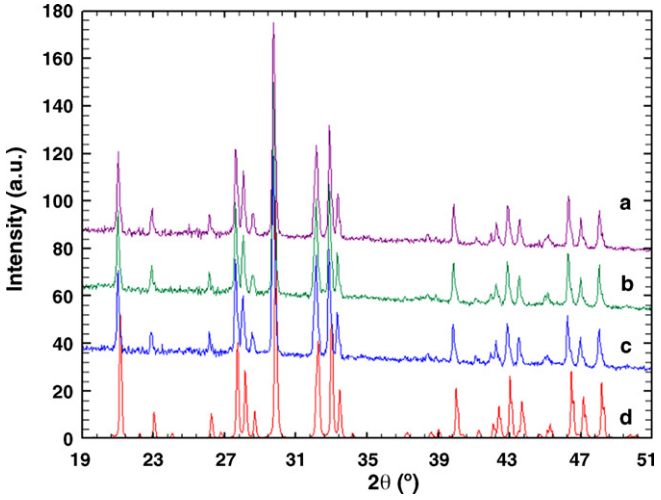

Fig. 1. The PXRD of the $La_2Ti_2O_7$ products prepared using (a) a 10:1 flux ratio heated for 10 h, (b) a 1:1 flux ratio heated for 1 h, (c) solid-state methods (1100 °C, 50 h), and compared to (d) the calculated theoretical pattern.

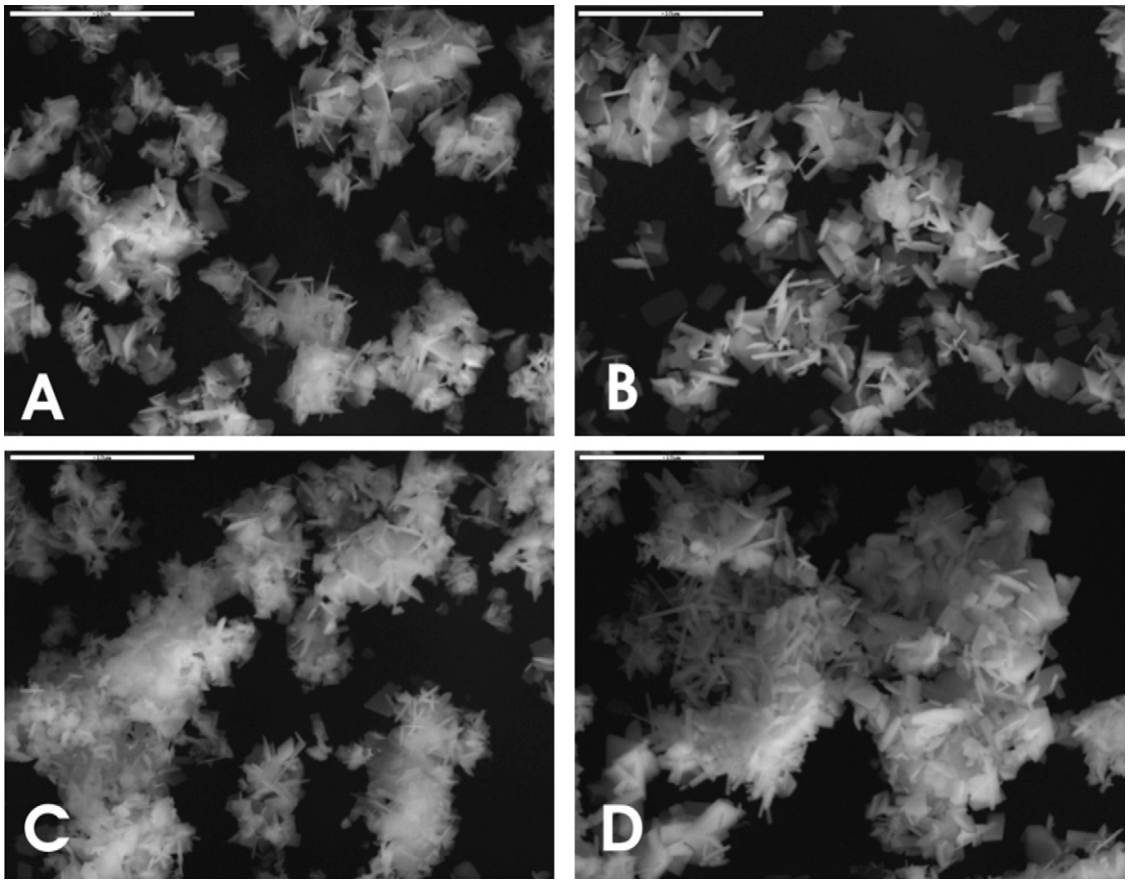

Fig. 2. SEM images of washed flux products for a 2:1 molar ratio of flux:$La_2Ti_2O_7$ after reaction times of (A) 1 h, (B) 2 h, (C) 5 h, and (D) 10 h. The scale is 10 μm.

with flux:$La_2Ti_2O_7$ ratios of 2:1 and 10:1 for reaction times of 1, 2, 5, and 10 h, shown in Figs. 2 and 3 respectively. These images reveal aggregations of distinct platelet-like particles of $La_2Ti_2O_7$, and which is typical of layered types of structures where the stacked perovskite layers correspond to the smallest crystal dimension. In this case, the top and bottom faces of the platelet particles would correspond to the (1 0 0) crystal faces, and the edges of the particles would correspond to the (0 1 0) and the (0 0 1) crystal faces. A distribution of platelet particle sizes was observed, with the lengths and widths of the platelets typically in the range of ~500–2000 nm for larger flux:$La_2Ti_2O_7$ ratios of 10:1 and 5:1 and ~1000–6000 nm for smaller flux:$La_2Ti_2O_7$ ratios of 2:1 and 1:1, as shown in Figs. 2 and 3. The measured average particle size for the smaller flux:$La_2Ti_2O_7$ ratio of 2:1 was 1068 nm in length and 200 nm in thickness, and for the larger flux:$La_2Ti_2O_7$ ratio of 10:1 was approximately 675 and 100 nm, respectively. While the individual particle sizes generally decreased both with increasing flux amounts and reaction time, a distribution of particle sizes could be found in all samples. A distribution of smaller particle sizes would most significantly enhance the number of exposed edges, i.e. the (0 1 0) and (0 0 1) crystal faces, while the amount of exposed (1 0 0) crystal faces would not be affected as significantly. Individual platelets were a few orders of magnitude thinner, down usually to <100 nm. The aggregation of the individual particles into larger agglomerates increased with increasing reaction times in each case, as shown in Figs. 2(C) and (D) and 3(C) and (D), but this was minimal with larger amounts of flux used in the synthesis. For comparison, SEM micrographs were taken of $La_2Ti_2O_7$ prepared by the solid-state method and compared to that obtained by flux synthesis, Fig. 4. The solid-state method yields neither a well-defined crystal morphology nor a range of distinct particle sizes. A calculation of the average particle size shows that $La_2Ti_2O_7$ samples prepared by the solid-state method show a rough particle size of approximately 320 nm. Nevertheless, the particle morphologies/microstructures are known to directly impact the photocatalytic activities of metal oxides [15,25,26]. Therefore, the flux synthetic technique offers a rapid and single-step approach to target more highly defined particle microstructures, as well as a more distinctive exposure of specific crystal faces that will be critical in probing their roles in photocatalytic properties.

Measurements of the UV–vis diffuse reflectance spectra were taken on all flux-synthesized $La_2Ti_2O_7$ samples in order to verify their optical bandgap sizes and as a probe of the averaged bulk particle sizes. These are shown for several selected samples in Fig. 5. The optical bandgap sizes were calculated from the onset of absorption using the well-known formula E_g (eV) = 1240/λ_g (nm), where λ_g (nm) is extrapolated from the linear rise in the absorption. In all cases, the optical bandgaps were calculated to be within a range of ~3.75–3.81 eV, and were in close agreement with previous studies [8,9].

The DRS of the $La_2Ti_2O_7$ samples prepared with a 5:1 flux ratio, Fig. 5(A), illustrate that the diffuse reflectance of sub-bandgap light (λ > 400 nm) increases with increasing reaction times of 1, 2, 5, and 10 h. A distribution of smaller particle sizes will increase the diffuse reflectance by enhancing the scattering and decreasing light penetration [19,20]. Thus, the averaged bulk particle dimensions show a clear trend towards smaller sizes with the 5:1 and 10:1 flux ratios with increasing reaction time, in agreement with the SEM images. However, for the smaller flux ratios of 2:1 and 1:1, the DRS do not increase regularly with increasing reaction time, e.g. showing a higher diffuse reflectance (and larger particle sizes) for 10 h

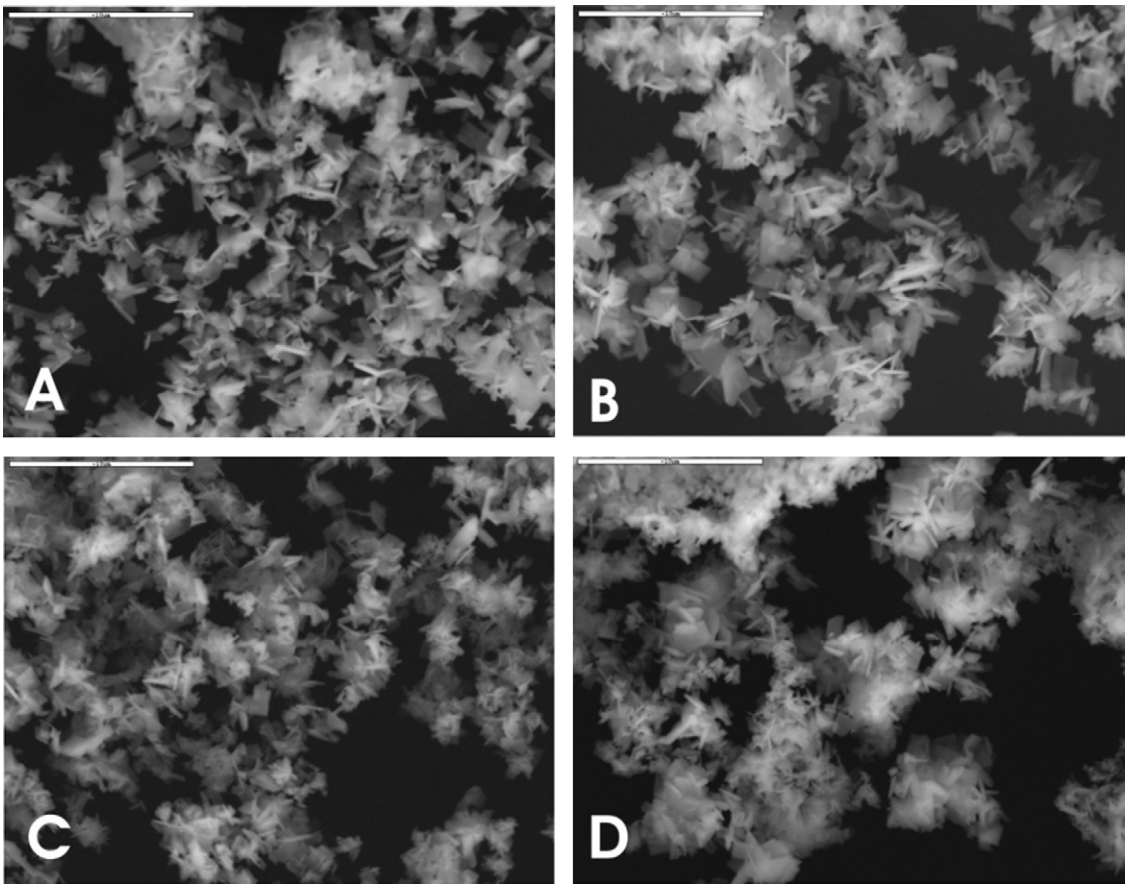

Fig. 3. SEM images of washed flux products for a 10:1 molar ratio of flux:$La_2Ti_2O_7$ after reaction times of (A) 1 h, (B) 2 h, (C) 5 h, and (D) 10 h. The scale is 10 μm.

versus 5 h. The smaller amounts of flux allow for closer interactions of the reactants and $La_2Ti_2O_7$ particles and for them to crystallize and grow via a solid-state rather than flux pathway. Thus, the larger amounts of flux are critical for the particles to be well separated. Both increasing amounts of flux and increasing reaction times yield the smallest particle sizes, as shown together in Fig. 5(B). For comparison, the UV–vis DRS of $La_2Ti_2O_7$ prepared via the solid-state method is also shown, and which has the lowest diffuse reflectance and the largest particle sizes.

The $La_2Ti_2O_7$ compound prepared by the solid-state method is among the most efficient photocatalysts reported, exhibiting quantum efficiencies of up to ~20–50%, depending on the dopants and surface co-catalysts [4,7]. Upon irradiation by bandgap or greater energies, the electrons that are excited into the conduction band serve to reduce water to H_2 at the Pt co-catalyst sites, while the photo-generated holes in the conduction band are scavenged by methanol to produce CO_2. The latter is used in order to measure the formation rate of H_2 alone, as the oxidation

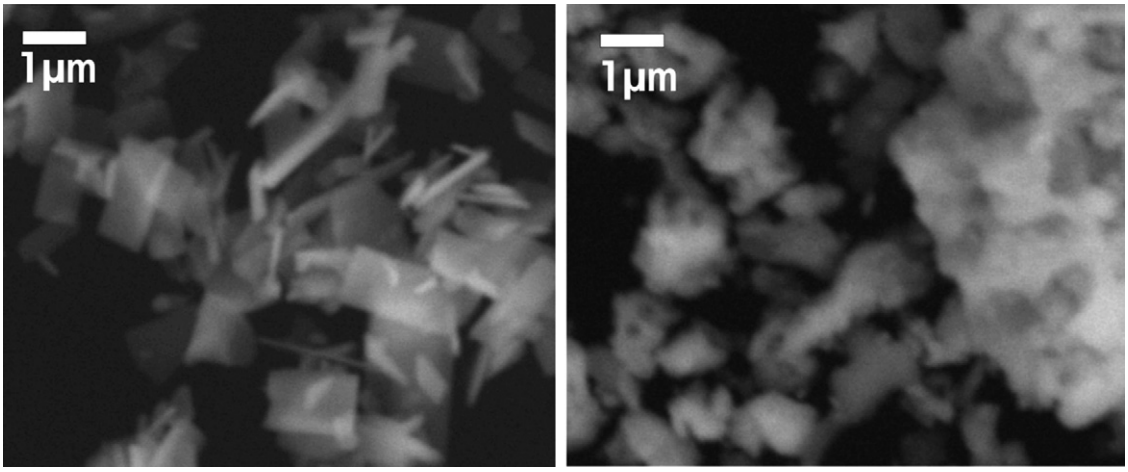

Fig. 4. Comparison of the SEM images of the particle morphologies obtained from a flux reaction (left; 10:1 ratio and 1 h reaction time) and from a solid-state preparation (right).

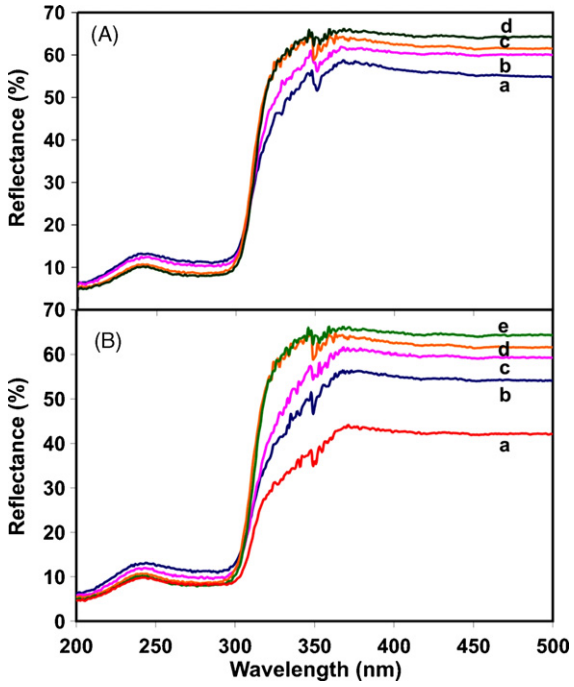

Fig. 5. Plots of UV–vis diffuse reflectance, as % reflectance versus wavelength, for (A) a 5:1 flux:$La_2Ti_2O_7$ ratio reacted for (a) 1 h, (b) 2 h, (c) 5 h and (d) 10 h, and (B) for the (a) solid-state sample and the flux samples of (b) 1:1 at 1 h, (c) 2:1 at 2 h, (d) 5:1 at 5 h, and (e) 10:1 at 10 h.

of water to O_2 can be slower and rate limiting. Flux syntheses of different particle-size distributions, as well as the different amounts of (1 0 0) and (0 1 0) or (0 0 1) crystal faces, can both potentially impact the rates of these surface reactions. Hence, the photocatalytic rates of H_2 production were measured for each $La_2Ti_2O_7$ sample under identical conditions, using ultraviolet irradiation in an outer-irradiation quartz reaction vessel in a 20% aqueous methanol or pure water solution. Listed in Table 1 are the reaction conditions and measured photocatalytic rates for the $La_2Ti_2O_7$ samples. The photocatalysis rates generally increased with increasing reaction times, with up to a 2–3× increase for flux

Table 1
Measured photocatalytic rates of hydrogen formation for $La_2Ti_2O_7$ prepared using a Na_2SO_4/K_2SO_4 flux and also by the solid-state method[a]

Sample	Synthetic conditions		Activity (μmol H_2 h^{-1} g^{-1})
	Flux:$La_2Ti_2O_7$ ratio	Time (h)	
$La_2Ti_2O_7$ std[b]	–	–	87
LTO1	1:1	1	55
LTO2	2:1	1	–
LTO3	5:1	1	58
LTO4	10:1	1	68
LTO5	1:1	2	80
LTO6	2:1	2	50
LTO7	5:1	2	30
LTO8	10:1	2	74
LTO9	1:1	5	87
LTO10	2:1	5	140
LTO11	5:1	5	119
LTO12	10:1	5	89
LTO13	1:1	10	138
LTO14	2:1	10	107
LTO15	5:1	10	99
LTO16	10:1	10	130

[a] Testing conditions: Outer irradiation 1000 W high-pressure Xe arc-lamp, 100 mg of $La_2Ti_2O_7$, 20% aqueous methanol solution, and 1 wt.% Pt surface co-catalyst.
[b] Prepared by solid-state reaction of TiO_2 and La_2O_3 reactants at 1100 °C for 50 h.

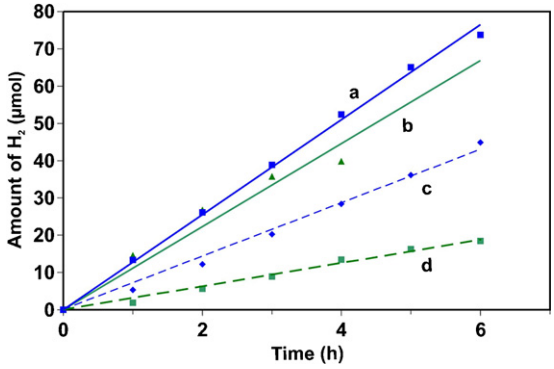

Fig. 6. Photocatalytic formation of hydrogen versus time for flux-synthesized $La_2Ti_2O_7$ prepared in a reaction time and flux:$La_2Ti_2O_7$ ratio of (a) 10 h and 10:1, (b) 5 h and 5:1, (c) 1 h and 10:1, and (d) 2 h and 5:1.

reactions at 10 and 5 h (~100–140 μmol H_2 h^{-1} g^{-1}) versus 2 or 1 h (~30–80 μmol H_2 h^{-1} g^{-1}). The higher rates therefore correlate with the smaller particle-size distributions and a higher number of exposed crystal edges and (0 1 0) and (0 0 1) surfaces, as confirmed by the SEM and DRS results (above). All $La_2Ti_2O_7$ samples prepared with a reaction time of 5 h or longer yielded rates higher than that exhibited by the sample prepared by the solid-state method, which exhibited a rate of 87 μmol H_2 h^{-1} g^{-1}. Shorter reaction times yielded lower rates than that of the solid-state sample. A comparison of the effect of both the flux amount and reaction time for the 10:1 and 5:1 samples is shown in Fig. 6, which is a plot of the total formation of H_2 versus time. The larger 10:1 ratio yielded much higher rates, compare blue versus green lines, while the shortest flux reaction times have lower rates in each case, compare the dotted versus solid lines. However, this illustrates that the reaction time has the more predominant effect on rates than the flux:$La_2Ti_2O_7$ ratio, which exhibited little discernible trends. This is likely the result of a range of particle-size distributions in every sample, as well as by partially solid-state driven reactions at the lower flux ratios of 2:1 and 1:1. The enhanced photocatalytic activities of the smaller and anisotropic platelet particles suggest that these platelet edges, i.e. orthogonal to the perovskite layer, are a significant factor in the high photocatalytic activity that had previously been observed for $La_2Ti_2O_7$.

For comparison, selected $La_2Ti_2O_7$ samples were tested in pure deionized water for photocatalysis. Each sample was loaded with a 1 wt.% Pt co-catalyst and placed in a reaction vessel with ~90 ml deionized water. Photocatalytic testing of both the solid-state sample and the 2 h 2:1 flux:$La_2Ti_2O_7$ sample showed no detectable activity after several hours of testing. The 10 h 10:1 flux:$La_2Ti_2O_7$ sample exhibited a rate of H_2 production in pure water of 31 μmol H_2 g^{-1} h^{-1}, averaged over ~12 h, and which was ~23% of its rate in an aqueous methanol solution. Thus, the smallest particles with the largest amounts of edges showed some of the highest activities in 20% aqueous methanol, and as well, their surfaces had been rendered active for hydrogen production even in a deionized water solution.

4. Conclusions

The rapid single-step synthesis of the (1 1 0) layered perovskite $La_2Ti_2O_7$ can be performed in a molten Na_2SO_4/K_2SO_4 flux at 1100 °C in short reaction times of 1–10 h. Platelet-like particle morphologies are obtained in high purity and with homogeneous microstructures that range in size from ~500 to 6000 nm, with thicknesses of <100 nm. The smallest particle-size distributions of ~500–2000 nm were obtained for increasing amounts of flux and

the longer reaction times of 5 and 10 h. Measured optical bandgap sizes of the $La_2Ti_2O_7$ products were in the range of ~3.75–3.81 eV. UV–vis DRS exhibited higher diffuse reflectances for the 10:1 and 5:1 samples for longer reaction times, i.e. for the samples with smaller particle sizes. Photocatalytic activities of the flux-synthesized $La_2Ti_2O_7$ samples in an aqueous methanol solution were ~55–140 μmol H_2 h^{-1} g^{-1}, with the maximum rates for the flux reactions time of 5 h or longer. The measured rates were nearly twice as large than for $La_2Ti_2O_7$ prepared by the solid-state method, and strongly suggest a key role of the crystallite edges and the (0 1 0) and (0 0 1) crystal faces in the origins of its high activity. Further, the flux-synthesized particles resulting from the highest flux ratios and reaction times were highly active for hydrogen production even in deionized water. Thus, flux synthetic preparations of $La_2Ti_2O_7$ particles have enabled a beginning of deeper insights into the surface features that govern its high photocatalytic activity.

Supporting information

UV–vis diffuse reflectance spectra of all flux-synthesized products, refined lattice parameters, and EDS results for composition analysis.

Acknowledgments

Support of this work is acknowledged from the Beckman Foundation through the Beckman Young Investigator Program (P.M.), and the Chemical Sciences, Geosciences and Biosciences Division, Office of Basic Energy Sciences, Office of Science, U.S. Department of Energy (DE-FG02-06ER06-15).

Appendix A. Supplementary data

Supplementary data associated with this article can be found, in the online version, at doi:10.1016/j.jphotochem.2008.06.005.

References

[1] M. Grätzel (Ed.), Energy Resources through Photochemistry and Catalysis, Academic Press, New York, 1983.
[2] H. Kato, A. Kudo, Catal. Today 78 (2003) 561–569.
[3] K. Domen, J.N. Kondo, M. Hara, T. Takata, Bull Chem. Soc. Jpn. 73 (2000) 1307–1331.
[4] J. Kim, D.W. Hwang, H.G. Kim, S.W. Bae, J.S. Lee, W. Li, S.H. Oh, Topics Catal. 35 (2005) 295–303.
[5] (a) K. Maeda, K. Teramura, D. Lu, N. Saito, Y. Inoue, K. Domen, Angew. Chem. Int. Ed. 45 (2006) 7806–7809;
(b) K. Maeda, K. Teramura, D. Lu, N. Saito, Y. Inoue, K. Domen, J. Phys. Chem. C 111 (2007) 7554–7560.
[6] D.W. Hwang, H.G. Kim, J. Kim, K.Y. Cha, Y.G. Kim, J.S. Lee, J. Catal. 193 (2000) 40–48.
[7] H.G. Kim, D.W. Hwang, J. Kim, Y.G. Kim, J.S. Lee, Chem. Commun. (1999) 1077–1078.
[8] D.W. Hwang, J.S. Lee, W. Li, S.H. Oh, J. Phys. Chem. B 107 (2003) 4963–4970.
[9] R. Abe, M. Higashi, K. Sayama, Y. Abe, H. Sugihara, J. Phys. Chem. B 110 (2006) 2219–2226.
[10] M. Uno, A. Kosuga, M. Okui, K. Horisaka, S. Yamanaka, J. Alloys Compd. 400 (2005) 270–275.
[11] D.W. Hwang, H.G. Kim, J.S. Lee, J. Kim, W. Li, S.H. Oh, J. Phys. Chem. B 109 (2005) 2093–2102.
[12] D.W. Hwang, H.G. Kim, J.S. Jang, S.W. Bae, S.M. Ji, J.S. Lee, Catal. Today 93–95 (2004) 845–850.
[13] J. Kim, D.W. Hwang, H.G. Kim, S.W. Bae, S.M. Ji, J.S. Lee, Chem. Commun. (2002) 2488–2489.
[14] D.W. Hwang, K.Y. Cha, J. Kim, H.G. Kim, S.W. Bae, J.S. Lee, Ind. Eng. Chem. Res. 42 (2003) 1184–1189.
[15] K. Li, Y. Wang, H. Wang, M. Zhu, H. Yan, Nanotechnology 17 (2006) 4863–4867.
[16] H. Song, T. Peng, P. Cai, H. Yi, C. Yan, Catal. Lett. 113 (2007) 54–58.
[17] J. Kim, D.W. Hwang, S.W. Bae, Y.G. Kim, J.S. Lee, Kor. J. Chem. Eng. 18 (2001) 941–947.
[18] H.G. Kim, D.W. Hwang, S.W. Bae, J.H. Jung, J.S. Lee, Catal. Lett. 91 (2003) 193–1193.
[19] D.G. Porob, P.A. Maggard, Mater. Res. Bull. 41 (2006) 1513–1519.
[20] D.G. Porob, P.A. Maggard, Chem. Mater. 19 (2007) 970–972.
[21] D.G. Porob, P.A. Maggard, J. Solid St. Chem. 179 (2006) 1727–1732.
[22] Z. Zhang, P.A. Maggard, J. Photochem. Photobiol. A 186 (2007) 8–13.
[23] J. Luo, P.A. Maggard, Adv. Mater. 18 (2006) 514–517.
[24] M. Gasperin, Acta Crystallogr. B 31 (1975) 2129–2130.
[25] C. Chang, Y. Zhu, Chem. Mater. 17 (2005) 3537–3545.
[26] H. Kato, K. Asakura, A. Kudo, J. Am. Chem. Soc. 125 (2003) 3082–3089.